Lasers in Manufacturing Conference 2017

Study on topology optimization design, SLM fabrication and performance of porous structure

Dongyun Zhang[a,b,*], Yangli Xu[a,b], Zhe Feng[a,b], Pudan Zhang[a,b], Xuanyang Cao[a,b]

[a]*Institute for Laser Engineering, Beijing University of Technology, Pinleyuan No.100, Chaoyang Dist., Beijing100124, China*
[b]*Beijing Engineering Reserch Center of 3D Printing for Digital Medical Health, Beijing International Cooperation Base for Digital Medical Health, Pinleyuan No.100, Chaoyang Dist., Beijing 100124, China*

Abstract

The combination of topology optimization (TOP) and Selective laser melting (SLM) provides the possibility to fabricate the complex, lightweight and of high performances of geometries. This paper evaluates the properties of porous structure with different porosity (40%~80%) and unite cell size (2~8mm), which are designed by topology optimization and explores their manufacturing limits for SLM. The compression properties, correlation between structural parameters (unit cell size and porosity) and dynamic elastic modulus of porous structure were investigated in properties evaluation. For manufacturing limits, three typical internal microstructures are abstracted and investigated including spiral structure, arched structure and structure with thin wall and small holes. During the compression experiment, these porous structures undergo catastrophic failure after forming crush band with an angle of 45°and their elastic modulus and compressive strength decrease with increase of both porosity and unite cell size. Gibson-Ashby model is used to evaluate the performance of porous structures, the value of structural parameter λ increases with the decrease of unite cell size indicating better stability of structure. Finally, the model for correlation between porous structural parameters and elastic modulus is established, which provides a mathematical reference for matching bone elastic modulus of different age, gender and skeletal site of human race.

Keywords: selective laser melting, topology optimization, porous structure, elastic modulus , compression behavior

* Dongyun Zhang. Tel.: +86-10-6739 6557; fax: +86-10-6739 2514.
E-mail address: zhangdy@bjut.edu.cn.

1. Introduction

Metal implants are in general used to replace defects and missing human bones. Although these traditional manufactured, dense metal implants cause some times a little issues and should pay more and more attention. Because it is dense and hence not conducive to the transport of water and nutrients (Hollister, 2009), metal implants may cause stress shielding (Langer and Vacanti, 1999), i.e. extrusion and preloading effects may exert greater pressure on the bone implantation process, leading to bone necrosis (Arabnejad *et al.*, 2016) and other problems. Porous material is a new type of innovative material. They have a high number of pores in it and can change the elastic modulus of the whole structure. The biological and mechanical properties of porous structure can be customized by their designed cells using special computer software. However, these complex porous structures are difficult to be precisely and successfully fabricated by traditional manufacturing method, selective laser melting (SLM), a kind of additive manufacturing method, is in consideration.

Porous titanium implants can improve the permeability and increase the ingrowth of bone cells (Langer *et al.*, 1990). But for application in a clinical setting, the porosity, pore size, and pore connectivity of porous materials should be appropriately selected and its properties should be evaluated. In recent years, the main design methods of porous structures include CAD-based design, image-based design, and implicit surface modeling. The diamond-like porous grids designed by CAD software have good mechanical stability due to their special structures (Ahmadi *et al.*, 2014), their elastic modulus is inversely proportional to the size of porous structure, strength cannot reach the application standard. The porosity of the image-based random foam is relatively large (76% ~ 87%), but a narrow range of elastic modulus (0.48 to 1.29 GPa), which has a certain distance for implants (Murr *et al.*, 2010). Porous structure characterized its intern shape and structure by implicit function model could be optimized to have the smallest contact surface, and even can overcome manufacturing limits of SLM (Giannitelli *et al.*, 2014). The strength is comparable to human bones, but the elastic modulus is not ideal.

Although the above design methods can construct relatively complex porous geometry model, especially the image-based design, with which can even get an internal trabecular structure, but its elastic modulus cannot be controlled and unable to be fabricated freely. Topology optimization is used to design the biological porous structure not only to ensure that it has sufficient rigidity and strength, but also make its elastic modulus to match the human skeleton (Chahine *et al.*, 2010). Some scholars have converted the design of 3D grid into 2D topological optimized grid, and the numerical analysis shows the gradient porous implants have better bone resorption (Khanoki and Pasini, 2012). XIAO et (XIAO *et al.*, 2012) used topology optimized porous structure to achieve the biomaterial and manufactured it using SLM, but related mechanical properties has not reported. The design of 3D topological optimized porous structure, manufacturing ability, mechanical properties and structural performance evaluation still need to be studied.

This paper evaluates the properties of porous structure with different porosity (40%~80%) and unite cell size (2~8mm), which are designed by topology optimization according to its stress condition and explores their manufacturing limits for SLM. In properties evaluation, the compression properties, correlation between structural parameters (unit cell size and porosity) and dynamic elastic modulus of porous structure are investigated. For manufacturing limits, three typical internal microstructures are abstracted out of design porous structures and investigated. Gibson-Ashby model is used to evaluate the performance of porous structures. Finally, the model for correlation between porous structural parameters and elastic modulus is established.

2. Experimental methods

2.1. Equipment and materials

The SLM samples are made on an EOS M280 equipment (manufactured by the German company EOS), which is equipped with an Yb-fibre 400 W laser with a 100 μm focal spot diameter. The scanning speed and layer thickness are respectively 7000 mm/s and 20–50 μm. The building volume (W × D × H) is 250 mm× 250 mm× 325 mm. The build chamber was backfilled with argon gas and the density of parts can be achieved above 98%. EOS Titanium Ti-6Al-4V (a titanium alloy powder) was used and its average size of the powder particles was 45 μm and an apparent density of 4.41 g/cm^3; the nominal composition of the gas atomized powder was Ti (85.7 wt. %), Al (6.75 wt. %), V (4.5 wt. %), the ingredients (balance).

2.2. Topology optimization design of porous unit cell

Topology optimization is used to optimize a structure for achieving lightweight and at same time maximum global stiffness. In the process of structure optimization, the structural model can be simplified as a cuboid; one of the vertices of which is subjected to a reverse force of 150 N along the Z-axis (arbitrary value), and its diagonal vertices are fixed. Structure parameter, such as elastic modulus of Ti-6Al-4V is 110 GPa, and the Poisson's ratio is 0.33. The objective function is the maximum structural rigidity design of restrainted by porosity, and set out the material distribution with porosity of 40%, 50%, 60%, 70%, and 80%. SOLIDWORK is used to reconstruct the model according to the profile of the Z-axis of the stress cloud. Magics 21.0 software is used to repair and smooth the surface of the unit cell. A complete lattice structure array is obtained by Boolean operation of the 1/8th unit cell with different porosity.

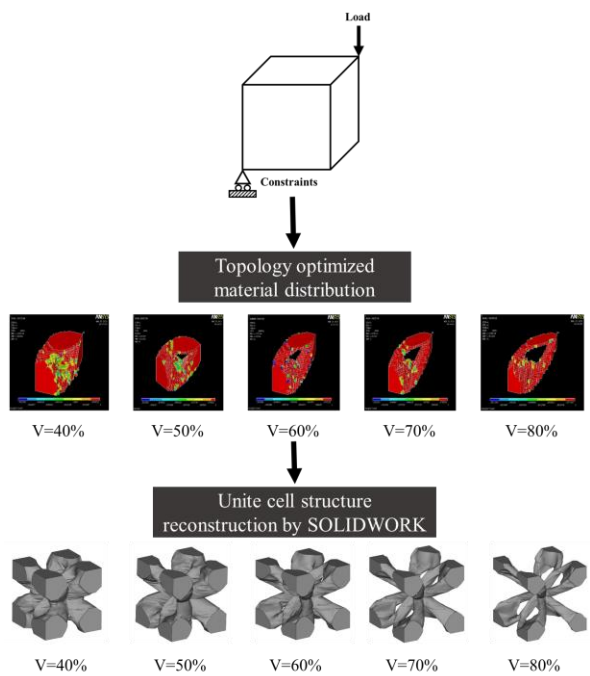

Fig. 1. The process of topology optimization and the result of unit cell model after 3D-reconstructure

2.3. Compression tests

The topology optimized unit cell for compression tests was used to generate two groups lattice structures: (1) with same porosity of 60% and various unit cell sizes of 1, 2, 3, 4 and 6mm, respectively; (2) with same unit cell size of 2mm and various porosity of 40%, 50%, 60%, 70% and 80% (fig. 2a and 2b), respectively. The compression tests were carried out using the German Zwick Roell equipment universal material sample machine (ZWICK/ROELL Z050) at room temperature. In order to get detailed information of structures crushing, the compression tests were monitored by a digital camera.

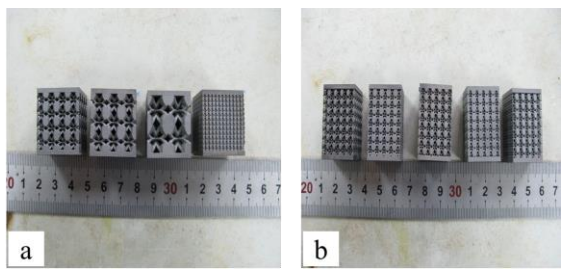

Fig. 2. Two groups of lattice structures manufactured by SLM for compression tests (a. with the same unit cell size of 2mm and various porosity of 40%, 50%, 70% and 80%; b. with same porosity of 60% and various cell sizes of 1, 2, 3, 4 and 6mm)

2.4 Measurement of porosity and elastic modulus

A series of porous structures with different porosity (40%~80%) and unite cell sizes (1~6mm) realized based on pile of unit cell by the Boolean operation and manufactured by SLM, the experimental porosity of the porous structure was measured by the mass method:

$$P = \left(1 - \frac{M}{V\rho_S}\right) \times 100\% \qquad (1)$$

Where P is porosity of porous structure, M is weight of sample (g) and V is spatial volume (including pore) of sample(cm^3). The weight is measured by electronic scales and the volume was determined by vernier caliper (V= length × width × height of porous lattice structure) and then calculated. ρ_S is material density of Ti-6Al-4V (i.e., 4.43 g/cm^3).

The dynamic elastic modulus of porous structures was determined using Analyzer RFDA from the Belgian company IMCE, by which the damping friction can be determined, too.

3. Result and discussion

Topology optimized geometry possesses lighter weight and at same time better working performances compared with the traditional designed one. But traditional manufacturing methods such as casting and forging encounter severe challenges due to the complexity of optimized geometry. SLM technology, as one of additive manufacturing methods, extends its manufacturing limit to the geometry with complex intern cavities and holes. The geometry with overhangs at the angle of 30° to the horizontal cannot be manufactured because of manufacturing limit of SLM, what should be investigated firstly because of its difference in materials and geometries. Furthermore, biomechanical properties of the porous Ti-6Al-4V structure should be tested whether they meet that of human bone. Meanwhile, the stability of topology

optimized porous structure and the relationship between structural parameters and elastic modulus would be discussed.

3.1. Manufacturability of topology optimization structure

Just as mentioned above, the complex geometry with especially intern structure such as sharp corners, inclined plane, holes, thin walls, overhang and so on should be paid more attention during fabrication with SLM. The manufacturing limit of SLM is different because of different SLM machine, materials and geometries to be fabricated. Three typical structures are abstracted out of the top optimized geometries, spiral structure（Fig.3a）, arched bridge structure（Fig.3b）, structure with thin wall and small holes（Fig.4c）, their manufacturing limits are investigated in the following.

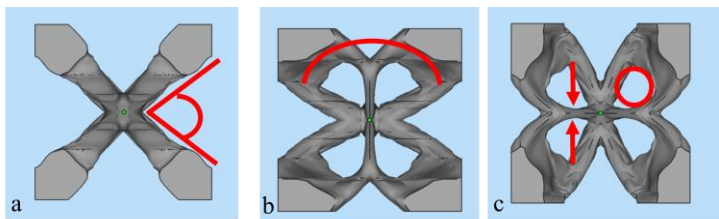

Fig. 3. Manufacture of structure of with angle, arched bridge structure, thin wall and small holes

3.1.1. Manufacturing limits of spiral structure

Three types of spiral structures with rising angle of 30°, 45° and 60° were investigated, respectively. The outside diameters of the base of spiral structures were 8 mm and that of spiral line were 2 mm. Three spiral structures were fabricated by SLM without supported structures generated using Magics Software. The results are shown in Fig 4.

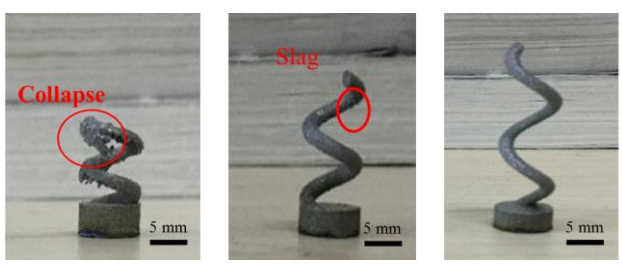

Fig. 4. Manufacturing limits and surface finish of spiral structures with rising angle of 60°, 45° and 30°

By contrast observation, the spiral structures with rising angle of 60° exhibited can be fabricated by SLM, the spiral line has a relatively smooth surface. The structure with rising angle of 45° also can be fabricated by SLM, however, slags were presented at the lower surface of spiral line, what worsens the surface finish of the spiral structure. The structure with rising angle of 30° occurs collapse exhibiting cannot be fabricated. Because the structure rise spirally up with the angle of 30°, which always collides with the recoater during SLM process, the fiercest collision is a head-on one just shown in Fig.5a when the rising direction of the spiral

structure is at a sharp angle of 30 ° to the direction of movement of recoater, the maximum frictional force between them occurs, the SLM fabrication process is stopped. On the contrary, the weakest collision occurs when the rising direction of the spiral structure is at an angle of 150° to the direction of movement of recoater just shown in Fig.5b. It normally locates between the two most friction values. If there unavoidably exits the possible fiercest collision in the structure to be fabricated, the supported structures should be generated for stiffness increasing of structure to be fabricated. Fig. 5c shows the manufacturing test specimen of spiral structure with rising angle of 30° with better surface finish.

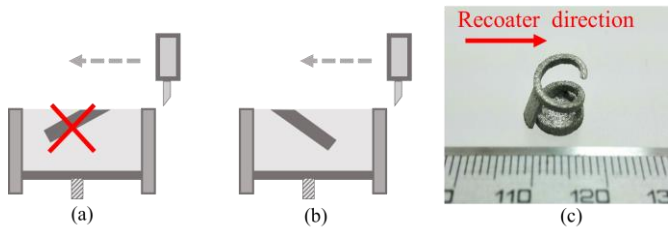

Fig. 5. 30°helical structure manufactured by SLM after adding some support

3.1.2. Manufacturing limit of the arched bridge structure

Manufacturability of a series of arched bridge structures with radius 2, 4, 6, 8, 10, 12, 14, 16 and 18 mm were investigated. When the radius of structure is greater than 10 mm, they cannot be fabricated because of collapse. When the structures with radius of 6, 8, 10 mm, they can be fabricated but the surface finish at the top of the arched bridge is worse. However, the structures with radius of 2, 4 mm can be fabricated even with better surface finish. From the experimental results, the greater is the radius of arched bridge structures, the larger is the overhang(Fig.6a), the more it collapses.

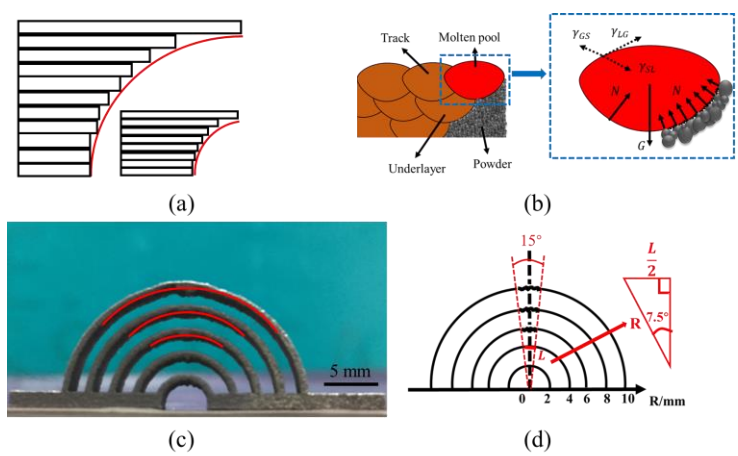

Fig. 6. (a) length of overhangs of arched structures with different radius during SLM process (b) the force acting on the liquid metal in molten pool (c) photos of arched bridge structure manufactured by SLM (d) the collapse area at the top of concentric circle varies with different radius of arched bridge structures

Just shown as in Fig. 6b, the force acting on the liquid metal in molten pool include surface tension, gravity and powder support from underlayer during SLM process. If the greater is the radius of arched bridge structures, the larger is the overhang, the more liquid metal in molten pool supported only by powder from underlayer, not by already solidified tracks. If the gravity of the molten pool is larger than the component of surface tension in the vertical direction, the support by powder from underlayer is not large enough to hold the liquid metal in molten pool, which penetrates into powder from underlayer and sinter to the lower surface (fig. 6c), seriously worsen the surface quality. Through observation and calculation, the penetration occurs at the top of concentric circle with radius of 2, 4, 6, 8, 10mm, respectively, i.e. it occurs inside the cone with cone angle of 15°, the top of cone is the center of concentric circle.

Therefore,

$$L_{max} \approx 2Rsin\theta = 2 \times 4 \times sin7.5° \approx 1.04mm \quad (2)$$

where R is the largest non-collapse radius, and θ is a half of cone angle of collapse area.
If the radius of arched bridge structures is large enough (larger than 10 mm), the gravity of the molten pool is most significant, the liquid metal of molten pool sinks directly and the collapse occurs, the SLM process can be stopped. Therefore, in the phase of structure design to be fabricated geometry, the length of the overhang should be controlled less than 1.04 mm for geometries with strict quality requirements, otherwise should generate support structure by Magics Software.

3.1.3. Manufacture of thin walls and small holes

Manufacturing limit of the structures with thin walls with thickness from 0.1 to 1 mm and small holes with diameter from 0.05 to 1mm was investigated (Fig. 7a). Comparison of design and measured values of thin walls and small holes is listed in table 1. As can be seen that the measured values of the thickness of thin walls are larger than that of design values, the measured values of the diameter of small holes are less than that of design values. The larger are the design values, the less the deviation between design value and measured value is.

The deviation between design value and measured value depends on the scanning strategies and beam offset value. During fabrication process of structures with thin walls using SLM, the laser scans firstly the contour of thin wall on powder bed and then scans the part of core. The contour line is the centreline of the laser and scanned track. The scanned track is larger than the laser spot size because of the existence of heat affected zone. So the measured values of the thickness of thin walls are always larger than that of design values, the measured values of the diameter of small holes are less than that of design values (Fig. 7b). The deviation value between design and measured value can be adjusted through change of beam offset value.

Table 1. Measurement parameters of the thin walls and the small holes

	Thin wall		Small hole	
	Theoretical value	Actual value	Theoretical value	Actual value
1	0.1	0.16	0.05	-
2	0.2	0.24	0.1	0.07
3	0.3	0.33	0.2	0.16
4	0.4	0.42	0.3	0.27
5	0.6	0.61	0.4	0.38
6	0.8	0.81	0.6	0.58
7	1.0	1.06	0.8	0.78
8	-	-	1.0	1.99

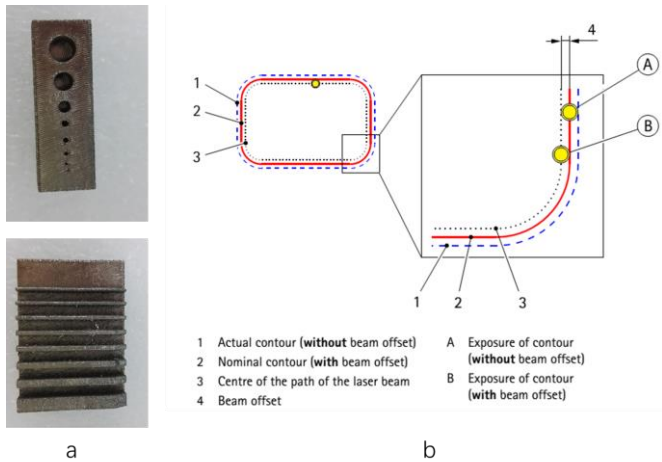

Fig. 7. (a). Samples of the thin walls and small holes, (b).beam offset on exposure of the contour.

3.2. Compression properties of the lattice structures

Table 2 lists the test results for elastic modulus and compressive strength of two groups of porous structures, one group with constant porosity of 60% and unit cell sizes from 1 to 6mm, and another group with constant unite cell size of 2mm and porosities from 40% to 80%, respectively. It is obvious that both properties tend to decrease with the increase of either unite cell size or porosities. The elastic modulus of porous structures are in the range of 4.02 and 34.20 GPa, while the corresponding compressive strengths are in the range of 48 and 320MPa. These results are also comparable to trabecular and cortical bones (Ryan and Williams, 1989, Choi *et al.*, 1990, Ashman *et al.*, 1984, Kuhn *et al.*, 1989). In comparison with other Ti-6Al-4V porous structure summarized by Cheng (Cheng *et al.*, 2012), the results suggest that topology optimized porous structure has better properties than the structure of CAD-based design.

Table 2. Compressive properties of optimized porous structures

Sample	Unite cell size, mm	Porosity, %	Elastic modulus, E (GPa)	Compressive strength, σ_b （MPa）
Lattice 1	1	60%	16.80	-
Lattice 2	2	60%	14.48	199
Lattice 3	3	60%	12.80	145
Lattice 4	4	60%	10.44	137
Lattice 5	6	60%	9.06	126
Lattice 6	2	40%	34.20	320
Lattice 7	2	50%	20.18	280
Lattice 8	2	70%	9.45	104
Lattice 9	2	80%	4.02	48
Trabecular bone	-	-	0.4~5.72	90~112
Cortical bone	-	-	6.9~21.5	125~172
X.Y.Cheng(2012)	-	62.08~91.65	0.19~6.34	3.8~112.8

The stress-strain curves from the uniaxial compression tests on the optimized porous structures with porosity of 60% and different unit cell sizes are shown in fig. 8. The results show clearly that they all have an elastic deformation region with a relatively high degree of linearity up to stress peak (AB), the slope of

middle region is the equivalent elastic modulus, which increase with the decrease of unit cell sizes. After that, a plateau region appears, in which the stress fluctuates excepting the porous structure with unit cell size of 1mm (BC). This can be attributed to the plastic deformation or failure of several beams of some porous structures, whereas others may be still in the elastic deformation region. Then the failure of porous structures occurred (CD) with the increase of strains, the crush bands expanded gradually from the top to bottom, and those bands formed at an angle of 45° with the axis(fig.9). Similar crush bands were also observed in typical porous structure (Zhang *et al.*, 2014) and reticulated mesh (Cheng et al., 2012). The fracture of dense metal normally prefers occur along the plane which has an angle 45° with the compressive direction. Finally, a densification region characterized by a rapid stress increase (DE).

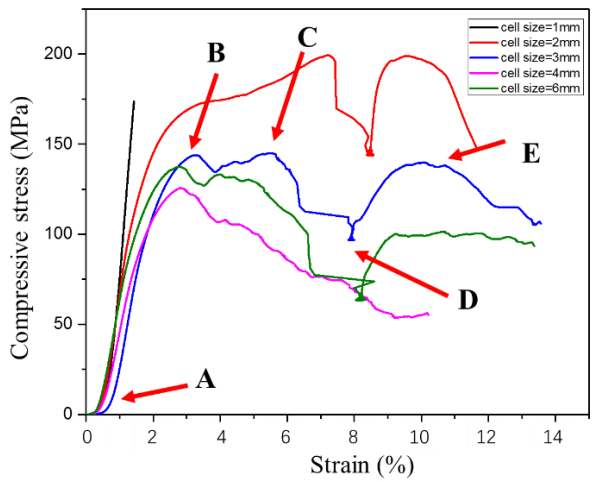

Fig. 8. Compressive stress-strain curve of 60% porosity optimized porous lattice structures with various unit cell sizes (1mm, 2mm, 3mm, 4mm and 6mm)

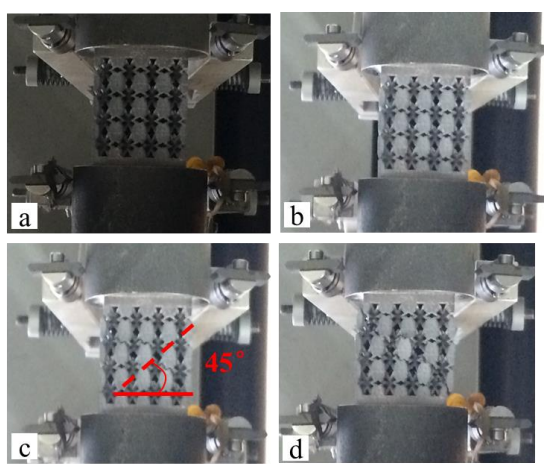

Fig. 9. Compressive deformation processes correspond to compressive stress-strain curve ((a) corresponds to fig. 8-AB, (b) corresponds to fig. 8-BC, (c) correspond to fig. 8-CD, (d) correspond to fig. 8-DE)

3.3. Evaluations of the porous structures

3.3.1. Measurement of dynamic elastic modulus

Table 3. Effective elastic modulus measured by RFDA

Unit cell size=1mm		2mm		3mm		4mm		6mm	
P[a] (%)	E[b] (GPa)	P (%)	E (GPa)	P (%)	E (GPa)	P (%)	E (GPa)	P (%)	E (GPa)
35.60	55.47	39.71	44.25	40.8	41.86	39.9	40.13	40.70	37.26
45.50	39.53	49.9	33.01	49.5	31.24	49.7	30.52	50.30	29.52
56.80	25.36	59.83	20.09	59.5	18.53	59.7	16.31	60.00	14.68
66.80	15.17	68.0	12.16	69.0	11.05	68.9	10.19	69.90	7.85
77.10	6.90	78.4	6.07	78.5	5.11	79.4	4.35	79.80	3.50

[a] Where P means the calculated value of porosity based on equation (1).
[b] Where E is effective elastic modulus of porous structures measured by RFDA.

The effective elastic modulus of porous structures with different unit cell sizes and porosities were measured by resonant frequency and damping analysis (RFDA) and illustrated in table 3. There is inverse relationship between effective elastic modulus and porosity and unite cell size, corresponding to the results of compressive test given in table 2. It worth to noting that these exists a little value difference due to the different measurement principle of two methods for elastic modulus of porous structures, in which RFDA is considered as a more accurate results as the integrity preserving of the internal structure of the porous lattice.

3.3.2. Evaluations of the porous structures

Structural performance evaluation of porous structure is based on the Ashby - Gibson model. Murr L E et al. proposed that the relative modulus (E/E_0) and the relative density (ρ/ρ_0) of open cellular structures satisfy the following relations:

$$\frac{E}{E_0} = \lambda\left(\frac{\rho}{\rho_0}\right)^n \quad (2)$$

Where E is the effective elastic modulus of porous structure, E_0 is the elastic modulus of fully dense material, ρ is the density of porous structure, ρ_0 is the material density value. Where λ is the geometric proportion constant, which can incorporate geometrical features or porous structures. In addition, the so-called effective elastic modulus for porous structures are priori calculated from equation (2) for n=2, especially for biomedical materials including Ti-6Al-4V. The relative density ρ/ρ_0 is obtained by equation (1):

$$P = \left(1 - \frac{m}{V\rho_S}\right) \times 100\% \left(1 - \frac{\rho}{\rho_S}\right) \times 100\% \quad (3)$$

$$\frac{\rho}{\rho_0} = 1 - P \quad (4)$$

Simultaneous equations (2) and (4):

$$\frac{E}{E_0} = \lambda(1-P)^2 \qquad (5)$$

Equation (5) is considered as structural performance evaluation model of porous structure. Plot the relative modulus (E/E_0) and the square of the relative density (ρ/ρ_0) according to data from table 3 is shown in fig. 10. The results show that the relative modulus and the square of the relative density follow a linear relation which fits with the theoretical model of the Gibson–Ashby. The slope of the straight lines is defined as the value of λ, of which the larger the value is, the more stable the structure is. Comparing with these results, the value of λ increases with the decrease of unite cell size of porous structure, indicating that it is not recommended to design biomedical implant using larger unit cell size.

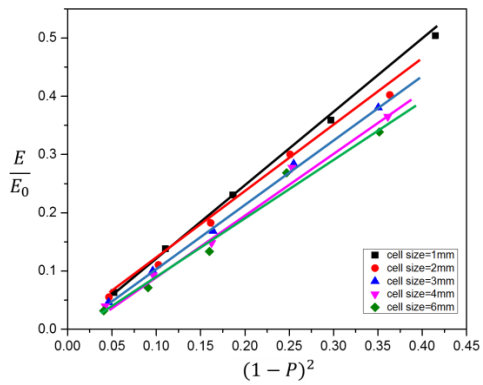

Fig. 10. The relative modulus (E/E_0) and the relative density (ρ/ρ_0) of open cellular structures vary with unite cell sizes (a-e correspond to 1, 2,3,4,6mm) illustrated in table 3

3.4. Evaluations of the porous structures

The result of fitting surface with the elastic modulus, the unite cell size and the porosity of topology optimized porous structure is shown in Fig. 11.

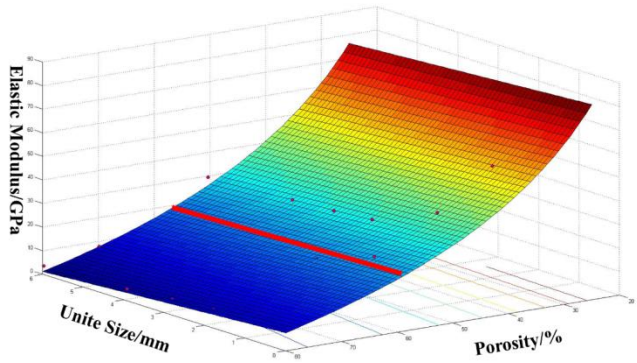

Fig. 11. Surface of porosity on Young's modulus

In order to obtain the elastic modulus (<21.5GPa) which matches the human body's bone and prevents the phenomenon of "stress shielding", the design range of elastic modulus for porous structures can be controlled by changing of unit cell size and the porosity. The requirements for porosity and unit cell size are selected below the red line (E=21.5GPa). Fitting the three parameters to obtain the equation:

$$E = -87.7892 - 1.077L + \frac{852.95}{P^{\frac{1}{2}}} \quad (6)$$

Where L represents unite cell size, P represents porosity, E represents the elastic modulus. The equation is obtained by a general-purpose global algorithm with a coefficient R^2= 0.9944, which is considered suitable as input for a production run. We can use this equation to obtain the relationship between the unit cell size and the elastic modulus of the porous structure, which is used to match the elastic modulus of different age, gender and bone position. Though it is useful for biomedical applications where a good controllability in terms of mechanical parameters is needed. However, future work is required to include different stress condition in different bone position.

4. Conclusion

Three aspects were investigated: the topology optimization design, fabrication using SLM and properties evaluation of porous structure. SLM technology, as a kind of most potential additive manufacturing methods, provides the possibility to fabricate porous structure with complicated intern shapes by overcoming manufacturing limit. The compression test showed the compressive strength and elastic modulus of topology optimized structures can match the requirements of trabecular and cortical bones of human race. The Ashby - Gibson model was used to evaluate the properties of porous structures indicating the better stability of the porous structure with smaller unite cell size. The model for parameters of porous structural and elastic modulus was established, and a detailed theoretical study about the model will be investigated including different stress condition in human bone position.

Acknowledgments

Thanks for the financial support from National Natural Science Foundation of China (Project No. 51675012).

References

Ahmadi, S. M., Campoli, G., Yavari, S. A., Sajadi, B., Wauthlé, R., Schrooten, J., Weinans, H. & Zadpoor, A. A. 2014, Mechanical behavior of regular open-cell porous biomaterials made of diamond lattice unit cells, Journal of the mechanical behavior of biomedical materials, Vol. 34106-115.

Arabnejad, S., Johnston, B., Tanzer, M. & Pasini, D. 2016, Fully porous 3D printed titanium femoral stem to reduce stress-shielding following total hip arthroplasty, Journal of Orthopaedic Research.

Ashman, R. B., Cowin, S. C., Van Buskirk, W. C. & Rice, J. C. 1984, A continuous wave technique for the measurement of the elastic properties of cortical bone, Journal of biomechanics, Vol. 17 No. 5, pp. 349-361.

Chahine, G., Smith, P. & Kovacevic, R. 2010, Application of topology optimization in modern additive manufacturing, in Solid Freeform Fabrication Symposium, pp. 606-618.

Cheng, X. Y., Li, S. J., Murr, L. E., Zhang, Z. B., Hao, Y. L., Yang, R., Medina, F. & Wicker, R. B. 2012, Compression deformation behavior of Ti–6Al–4V alloy with cellular structures fabricated by electron beam melting, journal of the mechanical behavior of biomedical materials, Vol. 16153-162.

Choi, K., Kuhn, J. L., Ciarelli, M. J. & Goldstein, S. A. 1990, The elastic moduli of human subchondral, trabecular, and cortical bone tissue and the size-dependency of cortical bone modulus, Journal of biomechanics, Vol. 23 No. 11, pp. 1103-1113.

Giannitelli, S. M., Accoto, D., Trombetta, M. & Rainer, A. 2014, Current trends in the design of scaffolds for computer-aided tissue engineering, Acta biomaterialia, Vol. 10 No. 2, pp. 580-594.

Hollister, S. J. 2009, Scaffold design and manufacturing: from concept to clinic, Advanced Materials, Vol. 21 No. 32-33, pp. 3330-3342.

Khanoki, S. A. & Pasini, D. 2012, Multiscale design and multiobjective optimization of orthopedic hip implants with functionally graded cellular material, Journal of biomechanical engineering, Vol. 134 No. 3, pp. 031004.

Kuhn, J. L., Goldstein, S. A., Choi, R., London, M., Feldkamp, L. A. & Matthews, L. S. 1989, Comparison of the trabecular and cortical tissue moduli from human iliac crests, Journal of orthopaedic research, Vol. 7 No. 6, pp. 876-884.

Langer, R. S. & Vacanti, J. P. 1999, Tissue engineering: the challenges ahead, Scientific American, Vol. 28086-89.

Langer, R., Cima, L. G., Tamada, J. A. & Wintermantel, E. 1990, Future directions in biomaterials, Biomaterials, Vol. 11 No. 9, pp. 738-745.

Murr, L. E., Gaytan, S. M., Medina, F., Lopez, H., Martinez, E., Machado, B. I., Hernandez, D. H., Martinez, L., Lopez, M. I. & Wicker, R. B. 2010, Next-generation biomedical implants using additive manufacturing of complex, cellular and functional mesh arrays, Philosophical Transactions of the Royal Society of London A: Mathematical, Physical and Engineering Sciences, Vol. 368 No. 1917, pp. 1999-2032.

Ryan, S. D. & Williams, J. L. 1989, Tensile testing of rodlike trabeculae excised from bovine femoral bone, Journal of biomechanics, Vol. 22 No. 4, pp. 351-355.

Xiao, D., Yang, Y., Su, X., Di, W. & Luo, Z. 2012, Topology optimization of microstructure and selective laser melting fabrication for metallic biomaterial scaffolds, Transactions of Nonferrous Metals Society of China, Vol. 22 No. 10, pp. 2554-2561.

Zhang, S., Wei, Q., Cheng, L., Li, S. & Shi, Y. 2014, Effects of scan line spacing on pore characteristics and mechanical properties of porous Ti6Al4V implants fabricated by selective laser melting, Materials & Design, Vol. 63185-193.